An Alternative Representation of the Ice Canopy for Calculating Microwave Brightness Temperatures over a Thunderstorm

BRADLEY M. MULLER, HENRY E. FUELBERG, AND ERIC A. SMITH

Department of Meteorology, The Florida State University, Tallahassee, Florida

18 May 1992 and 8 September 1992

ABSTRACT

Passive microwave brightness temperatures (T_B's) at 92 and 183 GHz from an aircraft thunderstorm overflight are compared with values calculated from radar-derived hydrometeor profiles and a modified proximity sounding. Two methods for modeling particles in the ice canopy are contrasted. The first is a "traditional" approach employing Marshall–Palmer ice spheres. The second, or "alternative," method partitions 20% of the ice water content into a Marshall–Palmer component for graupel and hail, and 80% into a modified gamma spherical particle size distribution function representing ice crystals.

Results from the alternative approach are superior to those from the traditional method in the anvil and mature convective core. In the decaying convective region, the traditional approach yields better agreement with observed magnitudes. Neither method, however, matches the geometry of the observed T_B depression associated with the decaying convective core. This is likely due to the presence of graupel, which is not detected as a special signature in radar reflectivity, but does diminish T_B's through scattering. Brightness temperatures at the relatively high microwave frequencies considered are shown to be very sensitive to the ice-particle size distribution.

1. Introduction

One of the most important factors influencing upwelling microwave (MW) radiances over thunderstorms is how the radiation interacts with frozen hydrometeors generated in the convective process. Vivekanandan et al. (1991) asserted that the ice phase may be the most inherently observable feature for scattering-based frequencies above 37 GHz. Therefore, accurate representations of ice–radiation interactions in forward radiative transfer calculations are a key element of physical remote data retrieval methods that use such frequencies. The spherical ice representation by Marshall and Palmer (1948, hereafter denoted M–P) is a "traditional" scheme used in the forward radiative transfer calculation for MW frequencies (e.g., Savage 1978; Wilheit et al. 1982; Spencer et al. 1983; Huang and Liou 1983). This note addresses an alternative methodology for calculations at 92 and 183 GHz. Specifically, we have incorporated a particle size distribution function (SDF) that accounts for ice *crystals* in addition to the M–P representation for precipitation-sized particles such as graupel and hail. Our purpose is to demonstrate the sensitivity of simulated upwelling brightness temperature T_B to simple SDFs of spherical particles for characterizing the ice canopy.

Corresponding author address: Bradley M. Muller, Department of Meteorology, The Florida State University, Tallahassee, FL 32306-3034.

Knowledge about the interactions between passive MW radiation and frozen hydrometeors has increased steadily since the 1970s. Using observations and modeling, Wilheit et al. (1982) were the first to demonstrate that scattering from precipitation-sized ice particles can account for extremely cold (140 K) T_B's at 92 and 183 GHz. Spencer et al. (1983) modeled similar signatures over land at 37 GHz. Aircraft overflights show that the 92- and 183-GHz frequencies are much less sensitive to anvil cirrus than are corresponding infrared measurements; however, scattering associated with large ice particles in active convective cores can produce T_B's over land that are much colder than any thermometric temperatures in the atmospheric column (Hakkarinen and Adler 1988; Adler et al. 1990; Heymsfield and Fulton 1988; Fulton and Heymsfield 1991).

Ice canopies affect top-of-atmosphere T_B through both their bulk and microphysical properties. For example, increasing the bulk ice concentration diminishes T_B's. On the other hand, particle density affects upwelling T_B through the complex index of refraction and particle size distribution (Smith and Mugnai 1989; Vivekanandan et al. 1990; Yeh et al. 1990a). These investigators showed that increasing density leads to decreasing T_B. Particle shape also has an effect, particularly as particle size and MW frequency increase. Modeling results indicate that the use of equivalent volume ice spheres can lead to errors in simulated T_B's; however, calculations of this impact are very computer intensive (Evans and Vivekanandan 1990). Neverthe-

less, there still exists a need for fast radiative transfer models in physical rainfall and other retrieval algorithms. This note describes an attempt to incorporate a spherical treatment for ice crystals into such models as an improvement over the M–P distribution.

Recent studies have begun to explore the important links between radar observations and passive MW data. Modeling results indicate that the 85- and 183-GHz channels "see" only the upper 3–5 km of optically thick clouds containing ice hydrometeors (Wu and Weinman 1984). Thus, aircraft measurements of T_B's at 92 and 183 GHz are well correlated with radar echoes from the upper portions of convective systems (Hakkarinen and Adler 1988; Heymsfield and Fulton 1988). Consequently, Yeh et al. (1990a) could simulate MW T_B's along an aircraft flight track by using vertical profiles of hydrometeor data derived from radar reflectivity as input to a radiative transfer model, thereby inferring information about particle size distribution and phase. Multiparameter radar measurements also have been used in both observational and modeling studies to characterize ice phase microphysics and its relationship to above-cloud microwave T_B's (Evans and Vivekanandan 1990; Vivekanandan et al. 1990; Vivekanandan et al. 1991; Fulton and Heymsfield 1991).

2. Methodology for comparing simulated and observed T_B's

We have employed the methodology of Yeh et al. (1990a) to compare AMMS (Advanced Microwave Moisture Sounder) T_B's from a thunderstorm overflight (Fulton and Heymsfield 1991) with calculations of passive microwave T_B at frequencies near 92 and 183 GHz. This flight occurred on 11 July 1986 during COHMEX (Cooperative Huntsville Meteorological Experiment). The T_B values were computed from a radar reflectivity cross section (Fig. 1) and a modified proximity sounding. Two methods were used to specify particle size distribution: 1) a "traditional" representation of radar-derived liquid and ice water content based on the M–P distribution; and 2) an alternative approach partitioning 80% of the ice content into a modified gamma distribution representing ice crystals

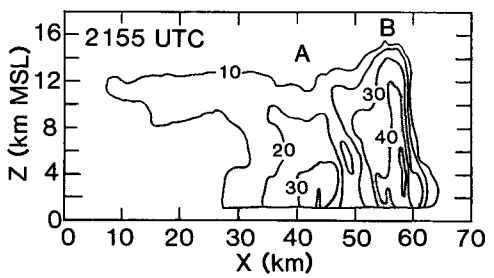

FIG. 1. Ten-centimeter radar reflectivity (dB) vertical cross section along the aircraft flight track. Flight direction was from 0 to 70 km. North is to the left (after Fulton and Heymsfield 1991).

(Welch et al. 1980), and 20% into M–P precipitation-sized particles such as graupel and hail. To our knowledge, previous calculations in the literature of MW T_B's from radar data have not explicitly accounted for scattering from a separate category of cloud ice crystals.

The AMMS (Wilheit et al. 1982) has frequencies in the window region at 92 ± 2 GHz and in the strong water vapor absorption line at 183.3 ± 9 GHz, 183.3 ± 5 GHz, and 183.3 ± 2 GHz. For computational efficiency, we adopted the approach of Kakar (1983) in modeling only one side of the two-sided AMMS channels at 90, 174.3, 178.3, and 181.3 GHz, and hereafter, refer to the channels by these values. Fulton and Heymsfield (1991) provide a full description and analysis of the radar and aircraft radiometric measurements used for this case.

The radiative transfer approach is based on a microwave version of Xiang's (1989) multilayer Sobolev solution to the radiative transfer equation. It is a plane-parallel two-stream multiple scattering solution for T_B that is comparable to an Eddington model (e.g., Wu and Weinman 1984) and has shown good accuracy when compared to multistream models. Yeh et al. (1990b) have demonstrated that an Eddington model can result in discrepancies compared with T_B calculations from a more sophisticated radiative treatment. The Sobolev model used here may suffer from similar limitations, which could account for some of the discrepancies between observed and calculated T_B's in section 3. An unpolarized version having 100 vertical layers and "viewing" at nadir was used here. Surface emissivity was set at 0.9. Optical parameters for polydisperse size distributions of spherical liquid and frozen hydrometeors were calculated for each layer using Wiscombe's (1980) Mie algorithm. For computational efficiency, lookup tables of these parameters were constructed based on temperature and liquid and ice water content (LWC and IWC). Gaseous absorption for each layer was calculated from the modified sounding using the algorithm of Liebe (1985).

The modified gamma SDF (Deirmendjian 1969) is given by Welch et al. (1980) as

$$n(r) = ar^{\alpha} \exp\left[-\frac{\alpha}{\gamma}\left(\frac{r}{r_c}\right)^{\gamma}\right], \qquad (1)$$

where $n(r)$ is the number concentration of droplets with radius r, and r_c is the modal radius (radius of maximum particle frequency). The modified gamma function yields a generic family of curves whose parameters r_c, a, α, and γ can be fit to actual particle distributions. Integrating the particle SDF and the volume formula with respect to radius gives LWC or IWC. A given size distribution can be scaled to a desired IWC by multiplying the particle number concentration in each radius category by the ratio of the desired IWC to the raw IWC. Thus, r_c remains constant, regardless of the final IWC. We used modified gamma parameters

for cirrus ice particles (Welch et al. 1980) with $r_c = 175\ \mu m$, $a = 4.0 \times 10^{-13}$, $\alpha = 5$, and $\gamma = 1.0$. This cirrus model represents the large particle mode of the bimodal distribution shown in Welch et al. (p. 44). They noted that typical ice-crystal lengths in cirrus might be three to five times those of equivalent spherical radii. Ice densities were set at 0.917 g cm^{-3}, that is, of pure ice. We contrast two types of T_B calculations: those for which all radar-derived liquid and ice water content is represented by the M–P SDF, versus those in which 80% of the ice content is represented by the modified gamma function for cirrus ice crystals, and 20% by the M–P SDF for hail and graupel.

The decision to partition ice mass into 80% "crystal" and 20% precipitation-sized components was somewhat arbitrary. Nevertheless, it reflects the fact that channels at 92 and 183 GHz are sensitive mainly to upper layers of the convective system, where crystals rather than precipitation-sized particles are expected to predominate. Applying formulas from Starr and Cox (1985), the assumed spherical mode radius of 175 μm can be compared with crystal lengths for particles of equivalent mass. Using our assumed ice density of 0.917 g cm^{-3} yields approximate crystal mode lengths of 1120, 775, and 910 μm for column, bullet rosette, and plate habits, respectively. These are in or near the range of mean particle sizes from 600 to 1000 μm reported by Heymsfield and Knollenberg (1972).

Vertical profiles of liquid and frozen water content were constructed from the 10-cm radar reflectivity cross section (Fig. 1) following the methodology of Yeh et al. (1990a). This employs Marshall and Gunn's (1952) modification of the classic Marshall and Palmer (1948) Z–R relation, with a correction for ice reflectivity (Smith 1984). The ice correction yields greater equivalent LWC than does the same reflectivity for liquid droplets. Given the radar reflectivity factor Z (mm^6 m^{-3}), the formula for LWC (g m^{-3}) is (Yeh et al. 1990a)

$$\mathrm{LWC} = aZ^b, \tag{2}$$

where $a = 0.00391$ and $b = 0.55$. The corrected formula for ice water content is

$$\mathrm{IWC} = 5.284aZ^b. \tag{3}$$

The factor 5.284 is equivalent to adding 7.2 dB to radar reflectivities expressed in decibels. Smith and Mugnai (1989) and Yeh et al. (1990a) have emphasized the importance of MW T_B calculations including a "mixed phase layer" of supercooled liquid drops and ice particles above the freezing level. Therefore, the proportion of ice to liquid water content has been assumed to increase linearly between 0.0° and −30°C. Sensitivity tests have indicated that this yields a positive impact at 90 GHz, but produces little or no change in the three 183-GHz frequencies.

Temperature and water vapor profiles within the thunderstorm depicted on the radar cross section were calculated from the proximity sounding released from Booneville, Mississippi, at 1845 UTC. The aircraft flight time was approximately 2155 UTC (1655 local daylight time). Saturated adiabatic ascent was assumed within the cloud starting at cloud base, with a dewpoint depression of zero within the cloud. At levels above the height at which radiosonde dewpoint information terminates, the environmental dewpoint depression was specified to be 30°C.

Heymsfield and Fulton (1988) and Yeh et al. (1990a) noted the potential for aircraft position errors due to drift in the inertial navigation system. Therefore, following Yeh et al., who used feature identification for matching radar cross sections with flight tracks, the aircraft measurements have been matched to the calculated T_B's by aligning very cold values in the convective core. This required an adjustment of 5 km.

3. Results and conclusions

Figure 1 is a vertical cross section of radar reflectivities along aircraft flight track 9 from Fulton and Heymsfield (1991). It was reconstructed from the volume scan occurring from 2155 to 2159 UTC, approximately concurrent with the T_B measurements. The aircraft was heading southward toward 70 km. Facing from 70 to 0 km along the cross section, the track is oriented approximately 15° to the right of the downshear vector, which we have estimated at approximately 325° from two-dimensional AMMS images. The storm motion vector is 250° at 11 m s^{-1} (Fulton and Heymsfield 1991). Three distinct features of this convective storm are relevant to our study: an anvil cirrus region from 7 to 30 km, a decaying convective core at 44 km (denoted by "A") with maximum low-level reflectivities over 40 dB, and a mature convective core near 58 km (denoted by "B") with maximum reflectivities exceeding 50 dB.

Figure 2 presents observed and calculated T_B's for the four AMMS channels. The calculated T_B's (denoted by "C") were based on the so-called traditional approach; that is, all hydrometeors were represented by the M–P SDF. The observed AMMS T_B's (denoted by "A") indicate anvil cirrus as a region of gently sloping values from 5 to 30 km along the flight track. The local minimum of observed T_B at about 39 km is associated with the decaying convective core, but is approximately 5 km downshear of the low-level reflectivity maximum. The coldest AMMS T_B's, ranging from 108 K at 174.3 GHz to 113 K at 178.3 GHz, are located near 57 km in conjunction with the mature convective core. Fulton and Heymsfield (1991) noted a hail signal in the multiparameter radar data for this region, indicating large ice particles that can cause significant scattering and, hence, very cold T_B's. Relatively warm T_B's, ranging from approximately 260 K at 181 GHz to 290 K at 90 GHz, are found upshear of the thunderstorm from approximately 60 to 70 km. Some low-level clouds occur in this region.

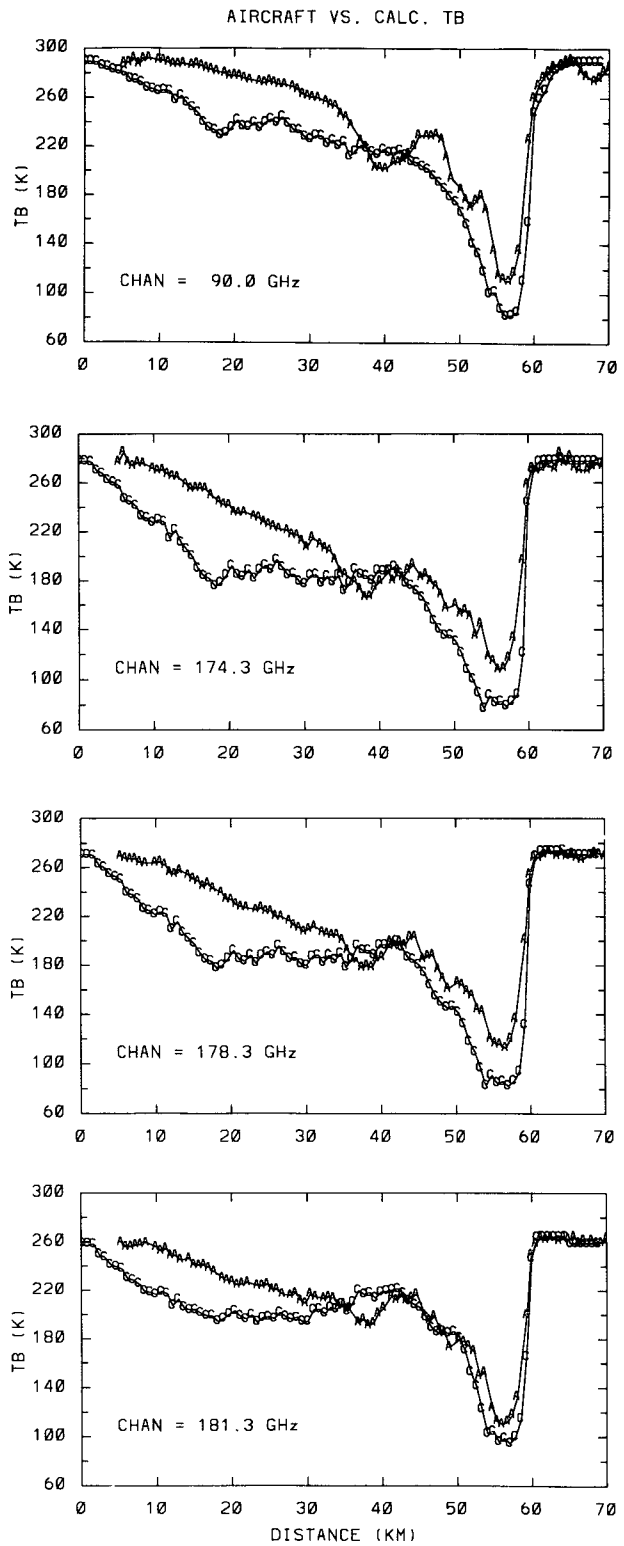

FIG. 2. Calculated T_B's (denoted by C's) and aircraft-measured T_B's (denoted by A's) for the four AMMS channels along the aircraft flight track. A "traditional" Marshall–Palmer particle size distribution representation for the ice water content was used.

Figure 3 repeats the observed AMMS T_B's from Fig. 2, but contains calculated values based on the 80%–20% partitioning of ice content into the modified gamma and M–P components. Except for the decaying convective region near 39 km and the results at 174 and 178 GHz in the mature core, the agreement between aircraft and simulated values is superior to the traditional 100% M–P representation. For example, T_B's in the anvil region calculated using the traditional method (Fig. 2) range from 20 to 60 K colder than observed for all four channels. Corresponding T_B's at 90 GHz calculated by the alternative method (Fig. 3), however, range from nearly equaling the AMMS values to approximately 10 K colder. The alternative T_B's at 174, 178, and 181 GHz also give closer agreements in the anvil region, but still average approximately 15 K too cold.

The main effect of applying the ice-crystal SDF while retaining some precipitation-sized ice hydrometeors (i.e., the alternative approach) is to increase the number of small particles, while at the same time decreasing the proportion of larger hydrometeors. The result is reduced scattering and warmer T_B's. Despite the T_B improvements, calculated values in the anvil still are too cold. There are several possible explanations for this result. As noted earlier, decreasing ice density can increase T_B's, and our value of 0.92 g cm^{-3} corresponds to that of pure ice, not the air–ice mixture that characterizes graupel and ice crystals. In addition, the assumption of saturated adiabatic vertical profiles of temperature and dewpoint within the radar echo region may overestimate water vapor content in the anvil region. Performance at 90 GHz is the best of the four channels in the area, perhaps because it is in a window region of the spectrum and is only minimally affected by water vapor absorption. Furthermore, even a 20% concentration of M–P ice spheres may place too many large ice particles in the anvil region. Tests using a 100% cirrus ice representation are shown for comparison in Fig. 4. Multichannel T_B agreements in the anvil from 5 to 20 km are better than those from the alternative approach. This is not true, however, in other storm regions. Thus, a 100% cirrus crystal scheme appears inappropriate for these areas.

The T_B's calculated by the alternative method (Fig. 3) are also an improvement over traditionally derived values (Fig. 2) in the mature convective core region near 57 km. For example, the traditional method gives T_B's that range from approximately 15 K too cold at 181 GHz to approximately 35 K too cold at 178 GHz. This method yields a mature core that is wider than observed at all frequencies. The alternative method, on the other hand, produces values that are nearly equal to those observed at 90 GHz, and are within 10 K at 181 GHz. It also appears to better capture the width and basic geometry of the observed T_B depressions.

Calculated T_B values at 174 and 178 GHz still are

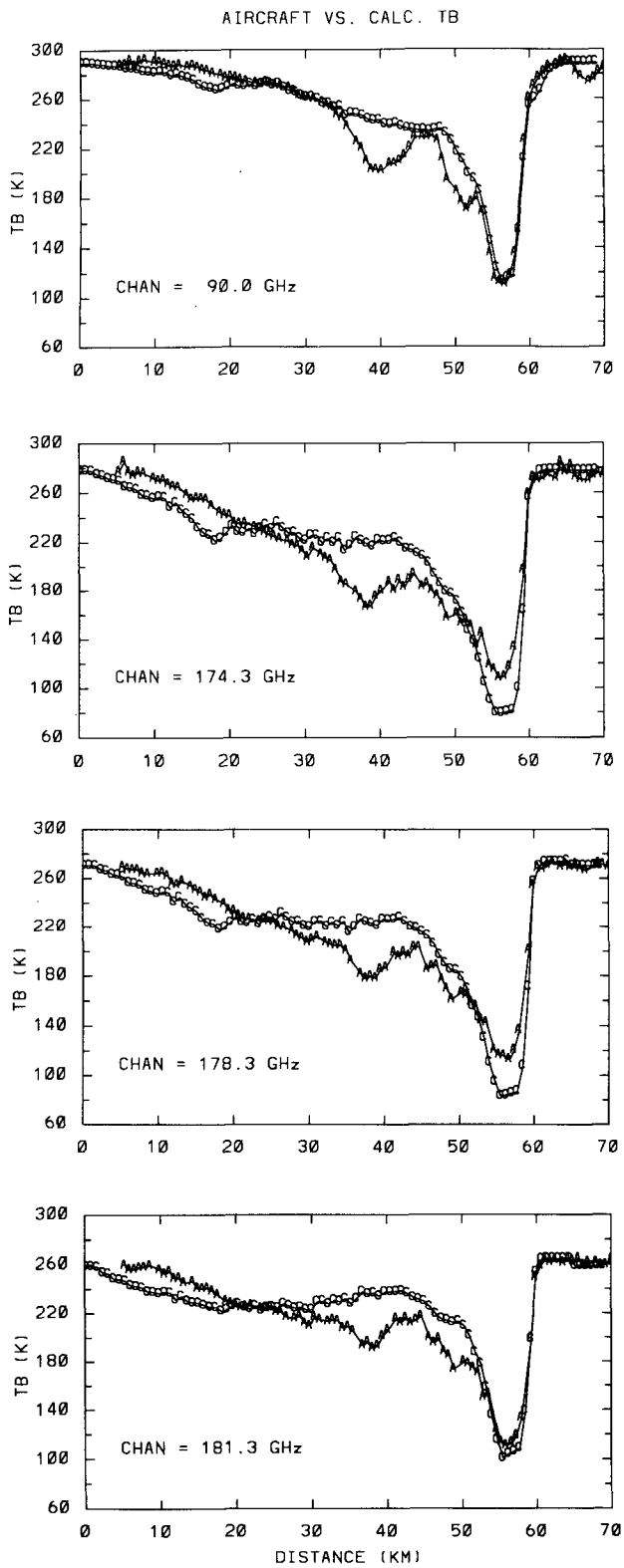

FIG. 3. Same as Fig. 2 but using an alternative approach with 20% of the ice water content represented by Marshall–Palmer spheres and 80% represented by modified gamma particle size distributions.

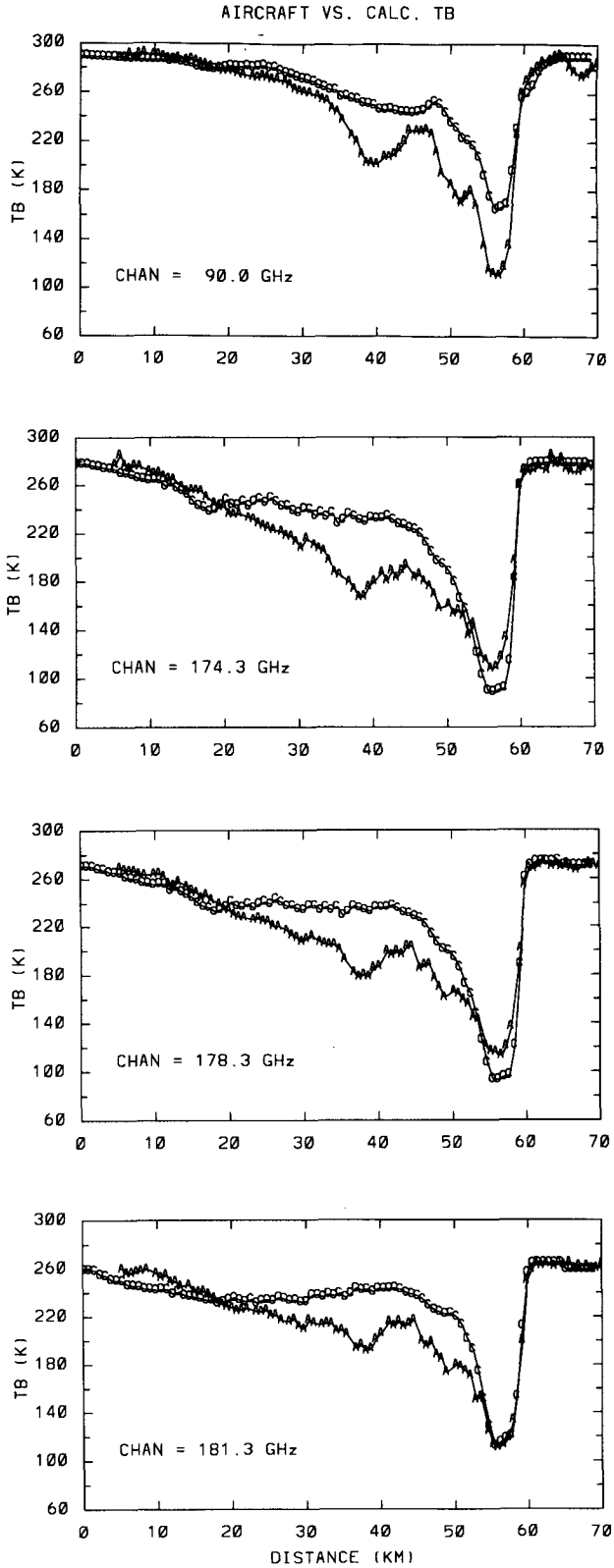

FIG. 4. Same as Fig. 2 but with 100% of the ice content represented by a modified gamma particle size distribution.

approximately 35 K too cold in the mature core, suggesting that errors remain in both the ice-particle distribution specification and the assumed water vapor profiles. The extremely cold T_B's imply that even the alternative approach overestimates scattering from ice particles at high microwave frequencies. In terms of its effect on T_B's, however, concomitant overestimation of water vapor profiles may compensate for errors in the ice specification, especially at 181 GHz. Channels nearest the center of the 183 GHz water vapor absorption line are most sensitive to upper-level water vapor. Thus, sensitivity studies (not shown) reveal that using a saturated adiabatic dewpoint profile, as employed in this work, adds 26 K of T_B at 181 GHz to that calculated using the unmodified environmental dewpoint profile. This procedure adds only 8 and 3 K, respectively, at 178 and 174 GHz.

Although the alternative methodology improved T_B's in the anvil and mature core, that is not the case in the decaying convective core near 39 km. Specifically, the traditionally derived T_B's (Fig. 2) are closer to observed values than those from the alternative procedure (Fig. 3). For example, traditionally calculated T_B's range from approximately 15 K warmer than the observed relative minimum at 90 GHz to nearly 30 K too warm at 181 GHz. The T_B's from the alternative approach are as much as 55 K too warm at 174 GHz. Neither method reproduces the geometry of the observed depression in T_B's. This may be attributable to large ice particles in the form of graupel, which are not indicated by the radar reflectivity signal. This hypothesis is supported by Fulton and Heymsfield (1991). Specifically, they show time series of AMMS T_B for an earlier storm in which a relative minimum of T_B occurs at the same time that radar reflectivities increase monotonically. This minimum is associated with an enhanced linear depolarization ratio signal from the multiparameter radar, suggesting the presence of graupel or aggregates of snowflakes. We speculate that a similar mechanism is operating here. In the current case it appears that the 10-cm radar reflectivity signal

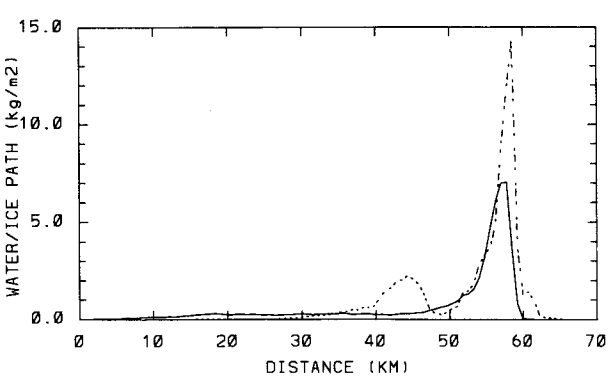

FIG. 5. Radar-derived columnar liquid water (kg m^{-2}, dashed) and ice "crystal" mass (kg m^{-2}, solid) along the aircraft flight track.

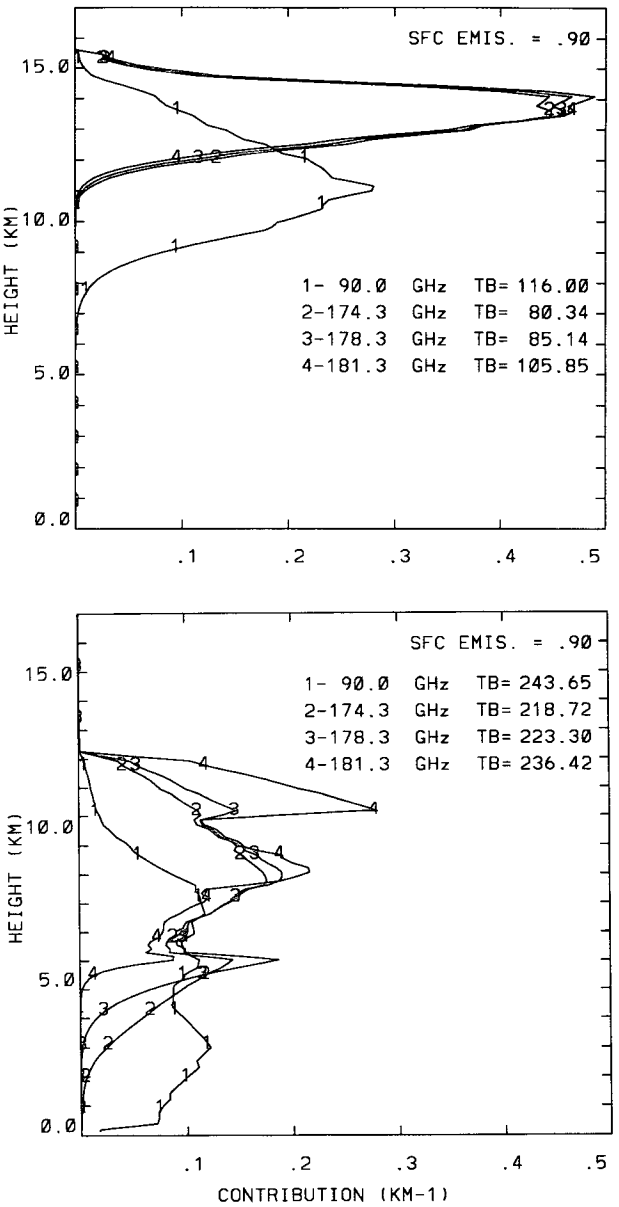

FIG. 6. Brightness-temperature contribution functions (km^{-1}) based on the alternative approach for the four AMMS channels in (top) the mature convective core and (bottom) the decaying convective core.

simply cannot distinguish between graupel particles to which the aircraft radiometer is highly sensitive and other forms of ice and liquid mass.

Radar-derived columnar liquid water and ice "crystal" masses along the aircraft flight track (Fig. 5) and T_B contribution functions (Fig. 6) for the mature and decaying convective regions help explain why the alternative method gives superior results in the mature core while the traditional approach yields better agreements in the decaying convective region. Values of precipitation-sized ice-particle mass have not been

plotted. The peak liquid water path in the mature core exceeds 14 kg m^{-2} (Fig. 5). The 7 kg m^{-2} of ice-crystal mass is located at higher levels of the storm. The sharp peaks of the contribution functions for the mature core (Fig. 6, top) near 14 km (about 170 mb) at 176, 178 and 181 GHz, and 11 km (about 250 mb) at 90 GHz suggest that the MW radiometer is "seeing" only the uppermost portions of the core. It seems likely that a proportion of precipitation-sized ice particles greater than 20% would be appropriate below the crystal layers, but their contribution is obscured from the satellite by the thick, mostly crystal canopy above. Therefore, the alternative approach works well for this region. In contrast, the ice-crystal mass in the decaying core (Fig. 5) is less than 0.5 kg m^{-2}, while the liquid water path for this region is 2 kg m^{-2}. Contribution functions for this area (Fig. 6, bottom) extend over a broad vertical portion of the storm. Thus, in this case, the 90- and three 183-GHz channels penetrate to layers in which the M–P representation appears more appropriate.

A final point concerns the close match between calculated and observed T_B's at 181 and 178 GHz between 65 and 70 km, that is, upshear of the storm (Figs. 2 and 3). These channels are most sensitive to mid- and upper-level water vapor. The relatively good agreement suggests that our arbitrary choice of a 30-K dewpoint depression above the last level of dewpoint information is reasonable for this region. The slight observed dip at 90 and 174 GHz is not reproduced in the calculated values. It may be attributed to lower-level clouds not seen in radar reflectivities but appearing in visible aircraft imagery (Fulton and Heymsfield 1991), or a surface emissivity fluctuation; it apparently is obscured by overlying water vapor at 178 and 181 GHz. Muller et al. (1992) have shown that channels near the center of the 183-GHz water vapor line receive little or no surface contribution in a clear atmosphere and that lower to middle clouds can be obscured by water vapor between them and the sensor.

In summary, inclusion of an 80% ice-crystal representation and a 20% M–P distribution gives overall results that are superior to the "traditional" approach for modeling aircraft measured T_B's in the anvil and mature convective core regions. In the decaying convective core region, however, the traditional approach, that is, 100% M–P distribution, gives better agreement. Neither method matches the geometry of the dip in T_B's in the decaying convective region. This is likely due to the presence of graupel, which is not detected as a special signature in radar reflectivities but does depress observed T_B's through scattering. To a significant degree, the 181- and 178-GHz channels are found to be sensitive to the upper-level water vapor profile.

Many previous authors have shown the importance of large ice particles for passive MW radiometry. The current work demonstrates that T_B's at relatively high MW frequencies are very sensitive to the particle size distributions. It emphasizes that particles smaller than those given by the conventional M–P SDF strongly affect the forward radiative transfer calculation, and therefore should be accounted for in physical retrieval schemes.

Acknowledgments. We gratefully acknowledge Richard Fulton of the NASA/Goddard Severe Storms Branch for providing the radar cross section and corresponding AMMS T_B data, and Dr. Mike Yeh for several helpful discussions. Dr. Steven Stage (FSU) provided some computer codes and Dr. Alberto Mugnai made useful comments. We greatly appreciate the assistance and suggestions of Dr. Franklin (Pete) Robertson of NASA/Marshall Space Flight Center (MSFC). Finally, we acknowledge the insightful comments and suggestions of three anonymous reviewers. This research has been supported by NASA/MSFC under the Graduate Student Researchers Program Grant NGT-50524.

REFERENCES

Adler, R. F., R. A. Mack, N. Prasad, H.-Y. M. Yeh, and I. M. Hakkarinen, 1990: Aircraft observations and simulations of deep convection from 18–183 GHz. Part I: Observations. *J. Atmos. Oceanic Technol.*, **7**, 377–391.

Deirmendjian, D., 1969: *Electromagnetic Scattering on Spherical Polydispersions.* Elsevier, 290 pp.

Evans, K. F., and J. Vivekanandan, 1990: Multiparameter radar and microwave radiative transfer modeling of nonspherical atmospheric ice particles. *IEEE Trans. Geos. Remote Sens.*, **28**, 423–437.

Fulton, R., and G. M. Heymsfield, 1991: Microphysical and radiative characteristics of convective clouds during COHMEX. *J. Appl. Meteor.*, **30**, 98–116.

Hakkarinen, I. M., and R. F. Adler, 1988: Observations of convective precipitation at 92 and 183 GHz: Aircraft results. *Meteor. and Atmos. Phys.*, **38**, 164–182.

Heymsfield, A. J., and R. G. Knollenberg, 1972: Properties of cirrus generating cells. *J. Atmos. Sci.*, **29**, 1358–1366.

Heymsfield, G. M., and R. Fulton, 1988: Comparison of high-altitude remote aircraft measurements with the radar structure of an Oklahoma thunderstorm: Implications for precipitation estimation from space. *Mon. Wea. Rev.*, **116**, 1157–1174.

Huang, R., and K.-N. Liou, 1983: Polarized microwave radiation transfer in precipitating cloudy atmospheres: Application to window frequencies. *J. Geophys. Res.*, **88**, 3885–3893.

Kakar, R. K., 1983: Retrievals of clear sky moisture profiles using the 183 GHz water vapor line. *J. Climate Appl. Meteor.*, **22**, 1282–1289.

Liebe, H. J., 1985: An updated model for millimeter wave propagation in moist air. *Radio Sci.*, **20**, 1069–1089.

Marshall, J. S., and W. M. Palmer, 1948: The distribution of raindrops with size. *J. Meteor.*, **5**, 165–166.

——, and K. L. S. Gunn, 1952: Measurement of snow parameters by radar. *J. Meteor.*, **9**, 322–327.

Muller, B. M., H. E. Fuelberg, and X. Xiang, 1992: Brightness temperature simulations for the physical interpretation of AMSU moisture channels. Preprints, *Sixth Conf. Satellite Meteorology and Oceanography.*, Atlanta, Amer. Meteor. Soc., 438–441.

Savage, R. C., 1978: The radiative properties of hydrometeors at microwave frequencies. *J. Appl. Meteor.*, **17**, 904–911.

Smith, E. A., and A. Mugnai, 1989: Radiative transfer to space through a precipitating cloud at multiple microwave frequencies. Part 3: Influence of large ice particles. *J. Meteor. Soc. Japan*, **67**, 739–754.

Smith, P. L., 1984: Equivalent radar reflectivity factors for snow and ice particles. *J. Climate Appl. Meteor.*, **23,** 1258–1260.

Spencer, R. W., W. S. Olson, W. Rongzhang, D. W. Martin, J. A. Weinman, and D. A. Santek, 1983: Heavy thunderstorms observed over land by the Nimbus 7 Scanning Multichannel Microwave Radiometer. *J. Climate Appl. Meteor.*, **22,** 1041–1046.

Starr, D. O'C., and S. K. Cox, 1985: Cirrus clouds. Part I: A cirrus cloud model. *J. Atmos. Sci.*, **42,** 2663–2681.

Vivekanandan, J., J. Turk, G. L. Stephens, and V. N. Bringi, 1990: Microwave radiative transfer studies using combined multiparameter radar and radiometer measurements during COHMEX. *J. Appl. Meteor.*, **29,** 561–585.

——, ——, and V. N. Bringi, 1991: Ice water path estimation and characterization using passive microwave radiometry. *J. Appl. Meteor.*, **30,** 1407–1421.

Welch, R. M., S. K. Cox, and J. M. Davis, 1980: Solar radiation and clouds. *Meteor. Monogr.*, No. 39, 96 pp.

Wilheit, T. T., A. T. C. Chang, J. L. King, E. B. Rodgers, R. A. Nieman, B. M. Krupp, A. S. Milman, J. S. Stratigos, and H. Siddalingaiah, 1982: Microwave radiometric observations near 19.35, 92 and 183 GHz of precipitation in Tropical Storm Cora. *J. Appl. Meteor.*, **21,** 1137–1145.

Wiscombe, W. J., 1980: Improved Mie scattering algorithms. *Appl. Opt.*, **19,** 1505–1509.

Wu, R., and J. A. Weinman, 1984: Microwave radiances from precipitating clouds containing aspherical ice, combined phase, and liquid hydrometeors. *J. Geophys. Res.*, **89,** 7170–7178.

Xiang, X., 1989: The Delta-Sobolev approach for modeling solar spectral irradiance and radiance. Ph.D. dissertation, School of Earth and Atmospheric Sciences, Georgia Institute of Technology, Atlanta, 178 pp. [Available from University Microfilms International, P.O. Box 1764, Ann Arbor, MI 48106.]

Yeh, H.-Y. M., N. Prasad, R. A. Mack, and R. F. Adler, 1990a: Aircraft microwave observations and simulations of deep convection from 18 to 183 GHz. Part II: Model results. *J. Atmos. Oceanic Technol.*, **7,** 392–410.

——, ——, ——, and R. F. Adler, 1990b: Tabulation of Mie properties for an effective microwave radiative model. *Meteor. Atmos. Phys.*, **42,** 105–112.